CCS Chemistry

RESEARCH ARTICLE

Received: Mar. 24, 2023 | Accepted: July 4, 2023 | Published: July 28, 2023

Design of Metal–Organic Assemblies via Shape Complementarity and Conformational Constraints in Dual Curvature Ligands

Cui-Lian Liu[1], Eduard O. Bobylev[2], Sébastien Dauriac[1], Brice Kauffmann[3], Koen Robeyns[1], Yann Garcia[1], Joost N. H. Reek[2] & Michael L. Singleton[1*]

[1]*Institute of Condensed Matter and Nanosciences, Université catholique de Louvain, Louvain-la-Neuve 1348,* [2]*Van't Hoff Institute for Molecular Sciences, University of Amsterdam, Amsterdam 1098 XH,* [3]*Université de Bordeaux CNRS, INSERM, UMS3033, Institut Européen de Chimie et Biologie (IECB), 33600 Pessac*

Corresponding author: m.singleton@uclouvain.be

Cite this: *CCS Chem.* **2023**, Just Published. DOI: 10.31635/ccschem.023.202302940

While common in biological systems, building blocks with low symmetry and flexibility pose numerous problems for synthetic self-assembly, such as the formation of isomers of assemblies that are difficult to distinguish and purify. In this work, three aromatic amide-based ligands (L1–L3) with a central 1,8-diazatriptycene core were designed and used for self-assembly with Pd^{2+}. While hundreds of stereoisomers based on the conformational flexibility around the amides and the unsymmetrical nonplanar structure of the core are possible upon coordination with the metal, the constraints designed into the ligands direct the self-assembly toward only a single Pd_2L_4 cage (L1) or Pd_4L_8 double-walled metallomacrocycle (L2) structure, even in mixtures of the ligands. This structural approach and the modularity of the ligand synthesis affords ready access to deep cavitands with endohedral functionalization (L3). These results highlight the potential of this new design strategy and open the door to selectively functionalized cavity-based architectures for numerous applications.

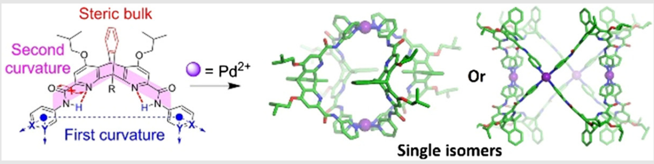

Keywords: **metal–organic cageopis, isomer selectivity, low-symmetry ligands, self-sorting, self-assembly**

Introduction

Self-assembly and folding play essential roles in the complexity and function of proteins.[1–3] In recent decades, the possibility of generating synthetic molecules with similar complexity and functions has inspired significant progress in the design of self-assembled cavitands.[4–12] While numerous strategies for the self-assembly of such structures have been developed, the combination of organic ligands and metal ions for the formation of metal–organic architectures has emerged as a highly promising approach.[13–18] Notably, the combination of Pd^{2+} or Pt^{2+} with ditopic ligands for the formation of M_nL_{2n} structures has attracted substantial attention and led to some of the largest well-defined systems.[19–21] A wide range of applications related to their cavities has been reported, including sensing, catalysis, drug delivery, storage, and molecular recognition.[22–29]

Unlike synthetic building blocks, the folding of peptides leads to subunits for self-assembly that have not only complex electrostatic potential surfaces but also a wide diversity of shapes.[30,31] The resulting high

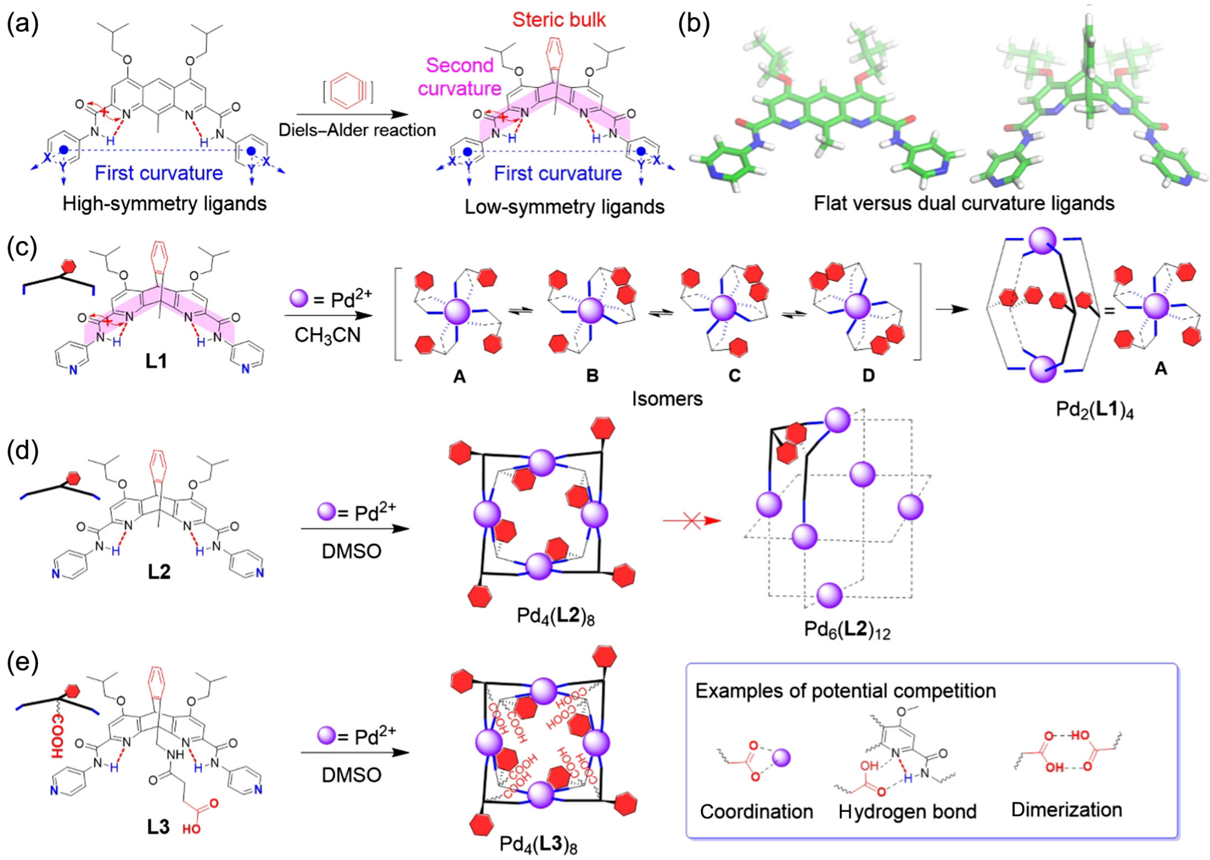

Figure 1 | *(a) Design of aromatic amide-based dual curvature ligands for coordination-driven self-assembly via Diels–Alder reaction with diazaanthracenes. This breaks the ligand symmetry and introduces additional shape complementarity as seen in the DFT-calculated structures of (b) flat versus dual curvature ligands. (c–e) The structure of ligands **L1–L3** and their self-assembled products. For (c), the cartoon for isomer A corresponds to the crystal structure shown in Figure 2e. The potential competitive interactions of the endohedral carboxylic acid are shown in the inset.*

complementarity between different subcomponents allows for the selective self-assembly of different units into complex asymmetric architectures. By contrast, the majority of synthetic strategies for coordination-driven self-assembly rely on rigid ligands with high, often planar, symmetry.[32] This can be readily seen in M_nL_{2n} assemblies. The ligands are most commonly curved organic molecules where *N*-heterocyclic donor groups are connected by flat aromatic or alkyne spacers, the rigidity of which allows the angle between coordination sites, the bend angle, to be well-defined.[14,33] This offers numerous advantages, such as allowing good prediction of the final self-assembled structures and clean formation of single species. Still, the use of lower symmetry ligands allows additional shape complementarity between ligands to help direct self-assembly, ultimately leading to new design strategies and more complex structures.[34,35] In the last decade, a number of elegant approaches relying on enhanced shape complementarity for controlling self-assembly have been described, such as combining two different ditopic ligands with compatible convergent and divergent bend angles or the use of coordination sphere engineering.[36–46] The latter uses additional functional groups included near the coordination sites on the ligands to provide complementarity through interligand steric or electrostatic interactions.[47–55] However, these approaches still largely rely on rigid or symmetric building blocks, with at least one of these properties usually being constrained to help direct self-assembly. Indeed, self-assembly with low symmetry and flexible building blocks is more challenging but represents an important approach to obtaining more complex and functional structures. For example, unprecedented topological nanostructures have been afforded through cooperative peptide self-folding and metal-induced self-assembly.[56–59]

Recently, we succeeded in using heteroaromatic amide-based ligands for the self-assembly of multiple Pd_nL_{2n} (*n* = 2, 6, or 12) metal–organic cages capable of neutral guest discrimination.[60] Despite the flexibility around the amide bonds, noncovalent interactions in the ligands lead to preferential folding into curved conformational states that orient the coordination sites and allow sufficient control over the bend angles of the ligands to direct self-assembly. Nevertheless, these

Citation: *CCS Chem.* **2023**, Just Published. DOI: 10.31635/ccschem.023.202302940
Link to VoR: https://doi.org/10.31635/ccschem.023.202302940

ligands are predominately flat and offer only limited interactions between ligands for the self-assembly of metal–organic cages. In fact, this is seen in the majority of ligands used for M_nL_{2n} assemblies.[19-21] Modification of the surface of the flat aromatic units to include perpendicular interactions is a challenge. However, this can be the fastest way to direct groups toward other ligands for designing interligand interactions and shape complementarity. We have recently shown that the large diazaanthracene[61] units used for our ligands are amenable to modification via the Diels–Alder reaction, leading to diazaiptycene or triptycene units.[62] These motifs are intriguing for incorporating additional shape complementarity aspects, remote from the coordination sites, into heteroaromatic amide ligands for self-assembly. In effect, the reaction of the central ring in the diazaanthracene bends the attached *N*-heterocyclic rings toward each other, a change which, in the ligand structure, adds an additional curvature perpendicular to the curvature that defines the bend angle (Figure 1a,b).

The design of such ligands with multiple curvatures for added shape complementarity has not been reported as a bottom-up strategy for metal–organic assemblies, and yet this approach could open up an opportunity for controlling self-assembly with even more complex components. Herein, we demonstrate that this dual curvature, combined with the electrostatic interactions that dictate the bend angle, can direct self-assembly towards a single M_2L_4 cage or M_4L_8 double-walled metallomacrocycle out of the myriad possible stereoisomers that result from different combinations of amide conformation and triptycene unit orientation (Figure 1b–e and Supporting Information Figures S1–S3 and S10). Importantly, this high isomer selectivity and self-sorting remain applicable, even when the ligands contain lateral functional groups that are competitive for metal binding or hydrogen bonding, allowing the further synthesis of deep cavitands with endohedral functionalization.

Experimental Methods

General experimental details

Unless otherwise stated, all chemicals and solvents were purchased from commercial companies and used without further purification. Fully detailed synthetic procedures for ligands **L1**–**L3** are described in the Supporting Information. ^1H and ^{13}C NMR spectra were recorded on a Bruker Biospin GmbH (Rheinstetten, Germany) AVANCE 500 MHz spectrometer or Avance II 300 MHz spectrometer at the Institute of condensed matter and nanosciences at the Université Catholique de Louvain. ^1H NMR chemical shifts are reported in ppm and determined with tetramethylsilane or calibrated against residual signals of the deuterated solvents. Deuterated solvents were purchased from Eurisotop (Saint-Aubin, France). High-resolution (HR) mass spectra were recorded by the mass spectrometry service of the Molecular Structural Analysis platform of the Institute of Condensed Matter and nanosciences at the Université Catholique de Louvain. Electrospray ionization time-of-flight mass spectrometry (ESI-TOF-MS) was collected on an HR-ToF Bruker Daltonik GmbH (Bremen, Germany) Impact II, an ESI-TOF-MS capable of a resolution of at least 40,000 full width at half maximum, which was coupled to a Bruker cryo-spray unit. Detection was in positive-ion mode, and the source voltage was between 4 and 6 kV. The machine was calibrated before every experiment via direct infusion of a sodium trifluoroacetate solution, which provided the *m/z* range of singly charged peaks up to 3500 Da in both ion modes. Data analysis was conducted with the Bruker Daltonik GmbH (Bremen, Germany) Data Analysis software, and simulations were performed with the Bruker Daltonik GmbH (Bremen, Germany) Isotope Pattern software. All computational models were constructed using initial semi-empirical calculations at the PM6 level with Gaussian 09[63] to optimize geometries of all structures before optimization using density functional theory (DFT). The resulting geometries were optimized with DFT calculations at the B3LYP/6-31G(d) level of theory for organic ligands and B3LYP/def2-SVP level of theory for metal-organic cages using Gaussian 09 package.[63]

Synthetic procedures

Self-assembly of $Pd_2(L1)_4(BF_4)_4$

A suspension of ligand **L1** (130.8 mg, 0.2 mmol, 1.0 equiv) and $Pd(CH_3CN)_4(BF_4)_2$ (44.4 mg, 0.1 mmol, 0.5 equiv) in 10 mL CH_3CN or dimethylformamide (DMF) was heated at 40 °C for 4 h. The turbid suspension of ligands gradually turned clear to give a yellow solution that was characterized by NMR to show formation of complex $Pd_2(\mathbf{L1})_4(BF_4)_4$. Diethyl ether was added to precipitate the isolated product $Pd_2(\mathbf{L1})_4(BF4)_4$. ^1H NMR (500 MHz, CD_3CN) δ 10.15 (s, 2H), 9.26 (ddd, *J* = 8.8, 2.2, 1.1 Hz, 2H), 8.57 (d, *J* = 2.3 Hz, 2H), 7.94 (d, *J* = 5.0 Hz, 2H), 7.64 (s, 2H), 7.50–7.44 (m, 4H), 7.05–7.01 (m, 1H), 6.90 (t, *J* = 8.1 Hz, 1H), 6.41 (s, 1H), 4.01 (dd, *J* = 21.3, 6.4 Hz, 4H), 2.76 (s, 3H), 2.22–2.19 (m, 2H), 1.12 (dd, *J* = 6.7, 2.2 Hz, 12H). ESI-TOF-MS for $Pd_2(\mathbf{L1})_4(BF_4)_4$.: The following picked signals are those at the high intensities. *m/z* calcd for $[M-2(BF_4^-)]^{2+}$, 1502.5008; found, 1502.5026; calcd for $[M-3(BF_4^-)]^{3+}$, 972.6657; found, 972.6660; calcd for $[M-4(BF_4^-)]^{4+}$, 707.7482; found, 707.7484.

Self-assembly of $Pd_4(L2)_8(BF_4)_8$

A solution of ligand **L2** (130.8 mg, 0.2 mmol, 1.0 equiv) and $Pd(CH_3CN)_4(BF_4)_2$ (44.4 mg, 0.1 mmol, 0.5 equiv) in 10 mL DMF or dimethyl sulfoxide (DMSO) was heated at 40 °C for 4 h to give a yellow solution that was

Citation: *CCS Chem.* **2023**, Just Published. DOI: 10.31635/ccschem.023.202302940
Link to VoR: https://doi.org/10.31635/ccschem.023.202302940

characterized by NMR to show formation of complex Pd_4(**L2**)$_8$(BF_4)$_8$. Diethyl ether was added to precipitate the isolated product Pd_4(**L2**)$_8$(BF_4)$_8$ from its DMF solution. ^{1}H NMR (500 MHz, DMSO-d_6) δ 10.83 (s, 2H), 9.10 (s, 4H), 8.12 (s, 4H), 7.50–7.58 (m, 4H), 7.15 (s, 2H), 6.28 (s, 1H), 4.02 (s, 4H), 2.65 (s, 3H), 2.10 (m, 2H), 1.05 (d, *J* = 6.5 Hz, 12H). ESI-TOF-MS for Pd_4(**L2**)$_8$(BF_4)$_8$: The following picked signals are those at the high intensities. *m/z* calcd for [M-3(BF_4^-)]$^{3+}$, 2033.0028; found, 2032.6786; calcd for [M-4(BF_4^-)]$^{4+}$, 1502.5008; found, 1502.5018; calcd for [M-5(BF_4^-)]$^{5+}$, 1184.7998; found, 1184.7991; calcd for [M-6(BF_4^-)]$^{6+}$, 972.8326; found, 972.8315; calcd for [M-7(BF_4^-)]$^{7+}$, 821.4273; found, 821.4265.

Self-assembly of $Pd_4(L3)_8(BF_4)_8$

A solution of ligand **L3** (153.8 mg, 0.2 mmol, 1.0 equiv) and $Pd(CH_3CN)_4(BF_4)_2$ (44.4 mg, 0.1 mmol, 0.5 equiv) in 10 mL DMF or DMSO was heated at 40 °C for 4 h to give a yellow solution that was characterized by NMR to show formation of complex Pd_4(**L3**)$_8$(BF_4)$_8$. Diethyl ether was added to precipitate the isolated product Pd_4(**L3**)$_8$(BF_4)$_8$ from its DMF solution. ^{1}H NMR (500 MHz, DMSO-d_6) δ 10.99 (s, 2H), 9.17 (s, 4H), 8.26 (s, 4H), 7.91–7.99 (m, 1H), 7.55 (m, 4H), 7.14 (s, 2H), 6.24 (s, 1H), 5.16(s, 2H), 4.03 (s, 4H), 2.36 (s, 2H), 2.24 (s, 2H), 2.11 (s, 2H), 1.04 (d, *J* = 6.4 Hz, 12H). ESI-TOF-MS for Pd_4(**L3**)$_8$(BF_4)$_8$: The following picked signals are those at the high intensities. *m/z* calcd for [M-4(BF_4^-)]$^{4+}$, 1732.5550; found, 1732.5381; calcd for [M-5(BF_4^-)]$^{5+}$, 1368.8432; found, 1368.8322; calcd for [M-6(BF_4^-)]$^{6+}$, 1126.2020; found, 1126.1941; calcd for [M-7(BF_4^-)]$^{7+}$, 953.0297; found, 953.0235. ESI-TOF-MS for Pd_5(**L3**)$_{10}$(BF_4)$_{10}$: *m/z* calcd for [M-7(BF_4^-)]$^{7+}$, 1212.9668; found, 1212.9580.

X-ray crystallographic details

The X-ray diffraction studies for complex Pd_2(**L1**)$_4$ and complex Pd_4(**L2**)$_8$ were carried out on a Rigaku (Rigaku Europe SE, Neu-Isenburg, Germany) FRX rotating anode (2.9 kW) diffractometer at the European Institute of Chemistry and Biology (Bordeaux, France) X-ray facility. Cu-K_α radiation monochromated with high flux Osmic Varimax mirrors were used for data collection. The X-ray source was equipped with a Dectris Ltd. (Baden-Dättwil, Switzerland) Eiger1M detector and partial chi goniometer. All crystals were kept at 130 K during data collection. CrysAlis^{Pr}[64] was used to index and integrate data with a multiscan absorption correction. Structures were solved with the ShelXT[65] structure solution program using Intrinsic Phasing and the structures were refined with the ShelXL[65] refinement package using Least Squares minimization within Olex2.[66] Only non-H atoms were refined with anisotropic displacement parameters. H atoms were positioned geometrically and constrained depending on their environment. Those H-atoms were refined in the riding-model approximation, with Uiso(H) = 1.2Ueq (CH, CH_2, NH). DFIX, AFIX, and RIGU restraints were applied to model geometry of the molecules and thermal motion parameters. The X-ray diffraction study for complex Pd_4(**L3**)$_8$ was carried out at a MAR345 image plate using Mo-K_α radiation generated by an Incoatex Microfocus source (focusing Montel multilayer opics ELM33) at UCLouvain. Prior to data collection, the crystals were flash-frozen to 120 K. Data integration and reduction were performed by CrysAlisPRO,[67] and the implemented absorption correction was applied. The structures were solved by SHELXT[65] and refined against F^2 by SHELXL-2018/3.[68] All nonhydrogen bonds were refined anisotropically, and hydrogen atoms were added in calculated positions and refined in riding mode, with temperature factors 1.2 times higher than their parent atoms. A full set of distance and angle restraints were used for the ligand, as well as planary restraints on the diazaanthracene units. Isotropic and rigid bond restraints were used on all nonmetal atoms. The crystal was found to be twinned by inversion with the twin ratio close to 50%. The crystal contained voids (61%) which were treated by the squeeze algorithm. Crystal data and structure refinement details are shown in the Supporting Information Table S1.

Results and Discussion

Ligand design and synthesis

Diazatriptycene ligands **L1** and **L2** were synthesized in three steps from the reported 1,8-diazaanthracene-2,7-dicarboxylate ester[61] (Scheme 1 and Supporting Information Figures S31–S33 and S66–S90), starting with a [4 + 2] cycloaddition between in situ generated benzyne. Subsequent saponification and amide coupling with either 3-aminopyridine or 4-aminopyridine gave ligands **L1** and **L2** in 68% and 87% yield, respectively. The Diels–Alder reaction with benzyne bends the ligands introducing the second curvature of ~120° between the planes of the amide groups based on the calculated structures (Figure 1a). Additionally, it adds a large benzene ring on one face of the ligand, which is expected to act as a source of steric hindrance between ligands to help control the self-assembly.

Self-assembly with L1 and L2

Complexation of **L1** with Pd^{2+} (NO_3^-, BF_4^-, $CF_3SO_3^-$, or PF_6^- salt) in a 2:1 molar ratio in CD_3CN or DMF-d_7 at 40 °C results in a clear yellow solution. After 2 h, the ^{1}H NMR spectrum shows a single sharp set of signals with the same number of resonances as the starting ligand (Figure 2a,b and Supporting Information Figures S4–S7, S91, and S92). Compared to **L1**, significant shifts of several resonances are observed. Notably, protons H_a

Citation: *CCS Chem.* **2023**, Just Published. DOI: 10.31635/ccschem.023.202302940
Link to VoR: https://doi.org/10.31635/ccschem.023.202302940

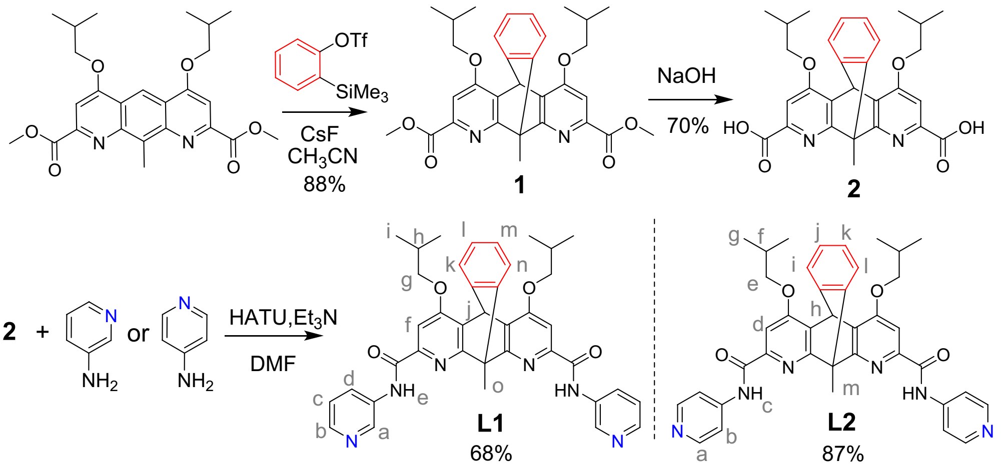

Scheme 1 | *Synthetic procedures for ligands **L1** and **L2**.*

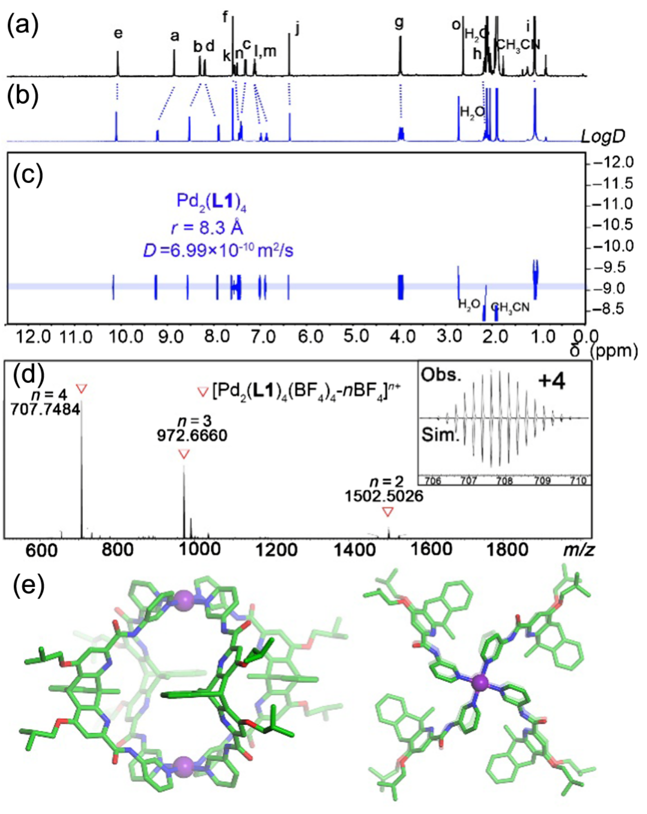

Figure 2 | *^{1}H NMR spectra (500 MHz, CD_3CN, 298 K) of ^{1}H NMR spectra of (a) **L1** and (b) its self-assembly product Pd_2(**L1**)$_4$. (c) The DOSY spectra of Pd_2(**L1**)$_4$. (d) ESI-TOF-MS for Pd_2(**L1**)$_4$ as its BF_4^- salt. Inset shows the comparison of the observed isotopic pattern with the simulated spectrum. (e) X-ray crystal structure of Pd_2(**L1**)$_4$ with views perpendicular to (left) and along (right) the Pd-Pd axis. Protons, solvent molecules, and counterions are omitted for clarity.*

and H_b of the pyridine groups appear further downfield, implying coordination of pyridine to Pd^{2+}. These observations suggest the formation of a single symmetric species derived from the complexation of **L1** with Pd^{2+} ions. Based on the expected parallel coordination vectors of the ligand, this was proposed to be an M_2L_4 structure. Consistent with this, diffusion-ordered ^{1}H NMR spectroscopy (DOSY) showed that all the proton resonances had the same diffusion coefficient of D = 6.99 × 10^{-10} m^2/s, which, based on the Stokes–Einstein equation, indicates a small structure with a radius of 8.3 Å (Figure 2c and Supporting Information Figure S25). ESI-TOF-MS further supported this assignment; a series of isotopic patterns corresponding to $[Pd_2(\mathbf{L1})_4(BF_4)_{4-n}]^{n+}$ (n = 2–4) were observed (Figure 2d and Supporting Information Figures S34–S37).

For this species, the symmetry and single set of signals observed by NMR are interesting because the different *syn/anti* orientations around the amides or *cis/trans* orientations of the ligand backbones lead to at least 528 possible stereoisomers (Figure 3 and Supporting Information Figures S8–S10). These nevertheless appear to converge to a single stable species, and time-dependent NMR studies of the self-assembly of **L1** did not show any clear signs of other isomers forming as intermediates (Supporting Information Figure S5). Within 10 min of mixing the ligand with Pd^{2+} ions, the ^{1}H NMR of the solution exhibited relatively broad signals with low intensity. ESI-TOF-MS analysis of the solution mainly found $Pd_2(\mathbf{L1})_4(BF_4)_4$, suggesting the composition of this mixture was predominately the M_2L_4 cage with possibly some oligomers and intermediates from the self-assembly. After 1 h, only a single sharp set of resonances, as observed above, emerges and becomes the significant species by ^{1}H NMR. In the presence of dimethyl sulfone as an internal standard, the observed signals account for >90% of the ligand used for self-assembly (Supporting Information Figure S7).

Citation: *CCS Chem.* **2023**, Just Published. DOI: 10.31635/ccschem.023.202302940
Link to VoR: https://doi.org/10.31635/ccschem.023.202302940

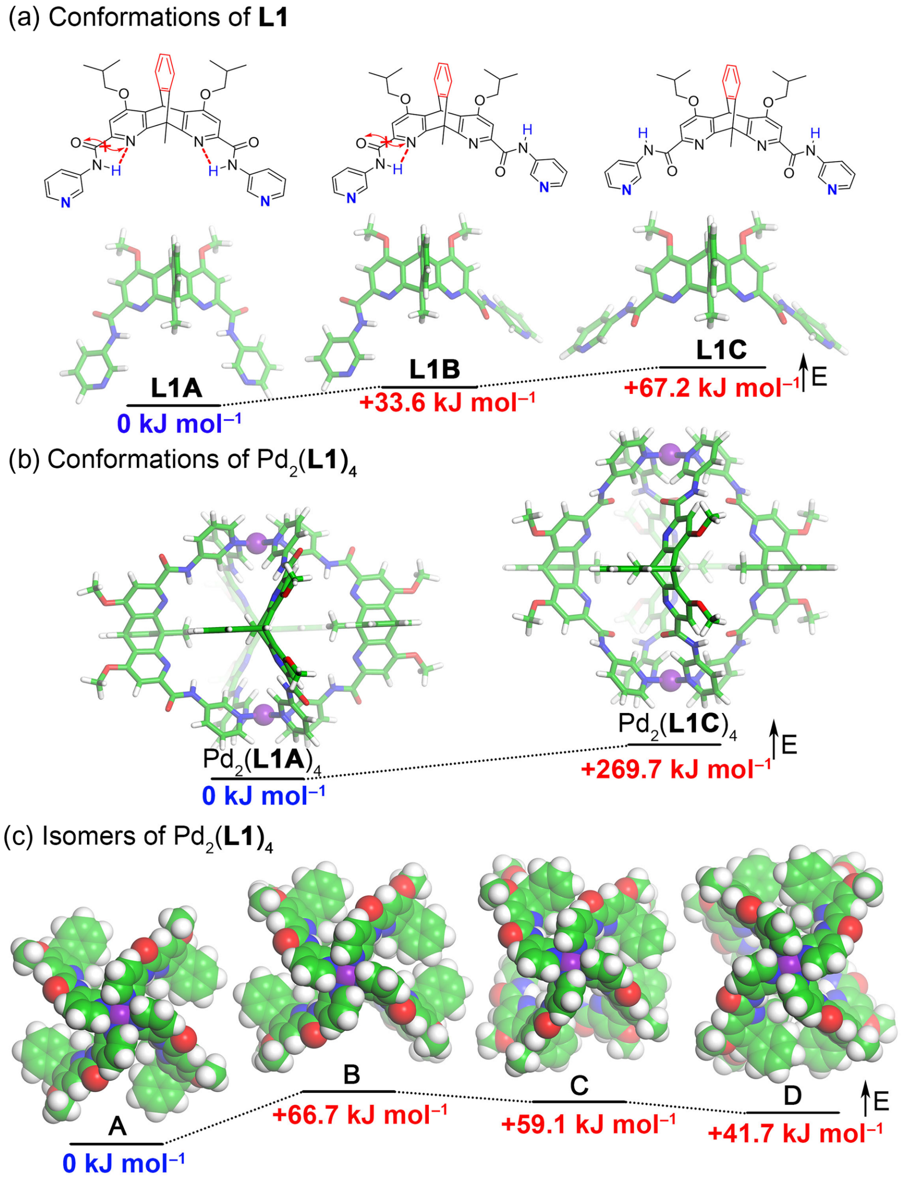

Figure 3 | *DFT-calculated structures and relative energies(B3LYP/6-31g* for ligands and B3LYP/def2SVP for cages) of (a) three possible conformations of ligand **L1**(**L1A**, **L1B** and **L1C**), (b) Pd_2(**L1**)$_4$ cage with representative ligand syn/anti amide conformations, and (c) four possible diastereomers of Pd_2(**L1**)$_4$ cage based on triptycene orientation.*

Relative to the possibility of different conformations, DFT computational studies (B3LYP/6-31g*) support that the *anti*conformation(**L1A**) between the amides of ligand **L1** (possible ligand isomers, **L1A**, **L1B**, and **L1C**) should be favored by almost 30 kJ/mol in the self-assembly solvent (CH_3CN) (Figure 3a). Similar studies (B3LYP/def2SVP) on the M_2L_4 cage also suggest that this preference should be maintained in the complex (Figure 3b). Still, the lack of planar symmetry in the ligands could result in four different Pd_2(**L1**)$_4^{4+}$ isomers (A–D) with different *cis/trans* relationships between the 9,10-bridging groups (Figure 3c). However, the dual curvature designed into the ligands should allow for good shape complementarity that directs single isomer formation in order to avoid steric interactions between neighboring ligands. Indeed, additional DFT studies comparing the four isomers estimated that isomer A, where the curves of the ligands are oriented in the same direction, should be the most stable by ~40 kJ/mol. Based on the calculated structures, the higher energy for the three other isomers likely results from steric interactions between nearby benzene rings in the diazatriptycene backbones.

Further support for the formation of isomer A came from its solid-state structure. Single crystals of Pd_2(**L1**)$_4$(BF_4)$_4$ could be obtained and were studied by X-ray diffraction (Figure 2e). The crystal structure of the complex shows two palladium ions, each in a square planar N_4 coordination environment, bridged by four

Citation: *CCS Chem.* **2023**, Just Published. DOI: 10.31635/ccschem.023.202302940
Link to VoR: https://doi.org/10.31635/ccschem.023.202302940

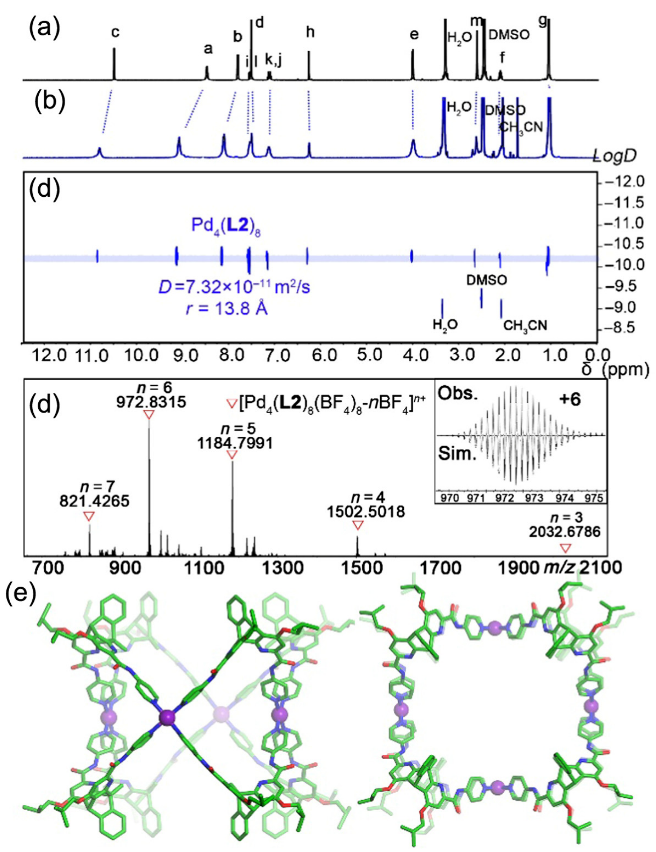

Figure 4 | *^{1}H NMR spectra (500 MHz, DMSO-d_6, 298 K) of ^{1}H NMR spectra of (a) **L2** and (b) its self-assembly product Pd_4(**L2**)$_8$. (c) The DOSY spectra of Pd_4(**L2**)$_8$. (d) ESI-TOF-MS for Pd_4(**L2**)$_8$ as its BF_4^- salt. Inset shows the comparison of the observed isotopic pattern with the simulated spectrum. (e) X-ray crystal structure of Pd_4(**L2**)$_8$ with side (left) and top (right) views. Protons, solvent molecules, and counterions are omitted for clarity.*

units of **L1** with a Pd^{2+}-to-Pd^{2+} distance in the cage of 12.3 Å. In accordance with the solution observations and computational results, the benzene rings on the ligands are all oriented in the same direction around the fourfold symmetry axis, and the amide carbonyls are all *anti* to the endocyclic nitrogens of the diazatriptycene units. Relative to our previously reported M_2L_4 cage,[60] which had overall D_{4h} symmetry, the directionality of the triptycene units used for Pd_2(**L1**)$_4^{4+}$ leads to a decrease in the symmetry of the cage to C_{4h}.

Motivated by the high selectivity observed with ligand **L1**, we next looked to see if the self-assembly of larger structures using the reduced symmetry ligands could still be controlled by the dual curvature effects. Ligand **L2** was reacted with 0.5 equiv of Pd^{2+} (NO_3^-, BF_4^-, $CF_3SO_3^-$, or PF_6^- salt) in DMSO-d_6 or DMF-d_7. Similar to self-assembly with **L1**, the ^{1}H NMR spectrum showed a single set of resonances distinct from the starting ligand (Figure 4a,b and Supporting Information Figures S11–S14, S93, and S94). Again, using an internal standard indicates that >90% of [**L2**] is represented by this new species (Supporting Information Figure S14). As expected, DOSY studies on this species suggested the formation of a larger structure (D = 7.32 × 10^{-11} m^2/s; r = 13.8 Å) (Figure 4c and Supporting Information Figure S26). However, as opposed to the M_6L_{12} or $M_{12}L_{24}$ cages obtained previously with the analogous planar ligand,[60] ESI-TOF-MS analysis showed isotopic patterns consistent with the formation of an M_4L_8 assembly with the formula Pd_4(**L2**)$_8$(BF_4)$_8$ (Figure 4d and Supporting Information Figures S38–S44). The M_4L_8 composition was further confirmed by X-ray diffraction studies. The crystal structure shows a deep crown-like double-walled metallomacrocycle (Figure 4e). The four palladium ions are found in the same plane and can be seen as occupying the four corners of a square. Each palladium has square-planar coordination, with two ligands, one above and one below the plane, bridging between each pair of adjacent metal ions. This gives a structure with cavity dimensions of 20.5 Å between opposite palladiums and 23.8 Å between the top and bottom faces. All of the ligands are oriented in the same way, with the benzene ring of the diazatriptycene units in each bridging pair pointing away from each other toward either the top or bottom of the structure. This also results in the 9-position group on the diazatriptycene units of the ligands converging towards the center of the cavity.

Interestingly, the bend angle for the ligands in the crystal structure of Pd_4(**L2**)$_8^{8+}$ is ~70°, while the same bend angle in the DFT optimized structure of the free ligands was found to be ~60°. Previously, we observed that the partial flexibility in the amide bonds could allow changes of almost 30° in the bend angle, making it possible to transition from a smaller cage structure to a larger one.[60] For example, M_6L_{12} and $M_{12}L_{24}$ structures, which require ideal bend angles around 90° and 120°, respectively, could be formed with the same aromatic amide ligand in a stepwise manner. With this in mind, we attempted to push the self-assembly of Pd_4(**L2**)$_8^{8+}$ toward a larger Pd_6(**L2**)$_{12}^{12+}$ octahedron. However, even after extending the time for self-assembly up to 2 weeks or increasing the temperature to 120 °C, no other apparent species were observed by NMR or ESI-TOF-MS analysis. The cube-like structures in most M_6L_{12} octahedra contain eight adjacent threefold symmetry axes. With the dual curvature ligand **L2**, it is impossible for the ligands to be arranged in a way where they are all pointing away from each other, something that can occur with Pd_4(**L2**)$_8^{8+}$ (Figure 4e). Interestingly, no close contacts of the complementary shapes, as seen in the isomers of Pd_2(**L1**)$_4^{4+}$, are observed in a PM6 model of a Pd_6(**L2**)$_{12}^{12+}$ octahedron (Supporting Information Figure S15). Thus, it is suspected that a combination of unfavorable ligand orientation and significant distortions in the torsion angles around the amides may limit the stability of the M_6L_{12} structure.

Citation: *CCS Chem.* **2023**, Just Published. DOI: 10.31635/ccschem.023.202302940
Link to VoR: https://doi.org/10.31635/ccschem.023.202302940

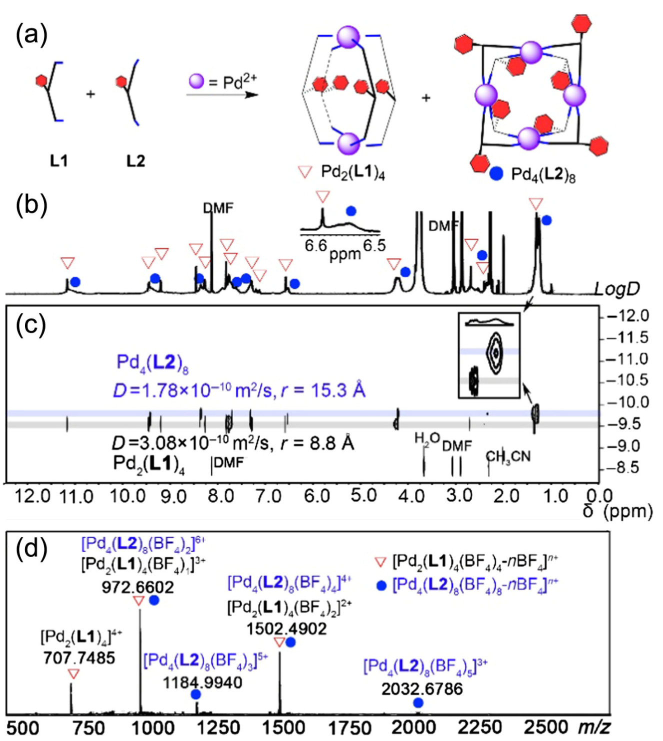

Figure 5 | *(a) Narcissistic self-sorting of M_2L_4 and M_4L_8 architectures from mixed ligands. (b) ^1H NMR spectra (500 MHz, DMF-d_7, 298 K), (c) the DOSY spectra, and (d) ESI-TOF-MS of self-sorting outcomes showing a mixture of M_2(**L1**)$_4$ and M_4(**L2**)$_8$ species.*

Self-sorting studies

To look at how strongly the noncovalent interactions present in the ligand structures control their bend angle, self-sorting studies were performed. In theory, changes in the torsion angles around the amides, at the expense of weakening the noncovalent interactions, should permit both ligands to achieve the same bend angles. While this could potentially allow the self-assembly of structures containing both ligands **L1** and **L2**, this does not appear to be favored, Figure 5a. Indeed, upon reacting a 1:1 mixture of **L1** and **L2** with $Pd(CH_3CN)_4(BF_4)_2$ in DMF-d_7, two distinct sets of signals corresponding to the M_2(**L1**)$_4^{4+}$ and M_4(**L2**)$_8^{8+}$ species as described above were observed by ^{1}H NMR (Figure 5b,c and Supporting Information Figures S20 and S28–S30). ESI-TOF-MS analysis, Figure 5d and Supporting Information Figures S51–S65, also showed only a mixture of M_2L_4 and M_4L_8 species. These observations indicate that, despite the weak nature of the noncovalent interactions that direct the ligand conformation, they still provide sufficient control to allow self-sorting based on the bend angle, something only previously reported for more ridged ligands.[69–71]

Cage functionalization

This shape complementarity strategy combined with the defined orientation of the diazaanthracene 9-position and modularity of the ligand design can facilitate the endohedral functionalization of the structure.[72] This enables us to look at the applicability of our strategy for self-assembly with a functional group that is potentially competitive with the metal coordination and noncovalent interactions important for the conformational stability. This can be especially interesting as there are still no reported examples of endohedral functionalized M_nL_{2n} type double-walled metallomacrocycles, mainly due to the fact that they require self-assembly from ditopic ligands with bend angles smaller than 90°, which limits endohedral functional sites. To this end, ligand **L3** bearing a carboxylic acid function was synthesized, as shown in Scheme 2. Following reported procedures, the

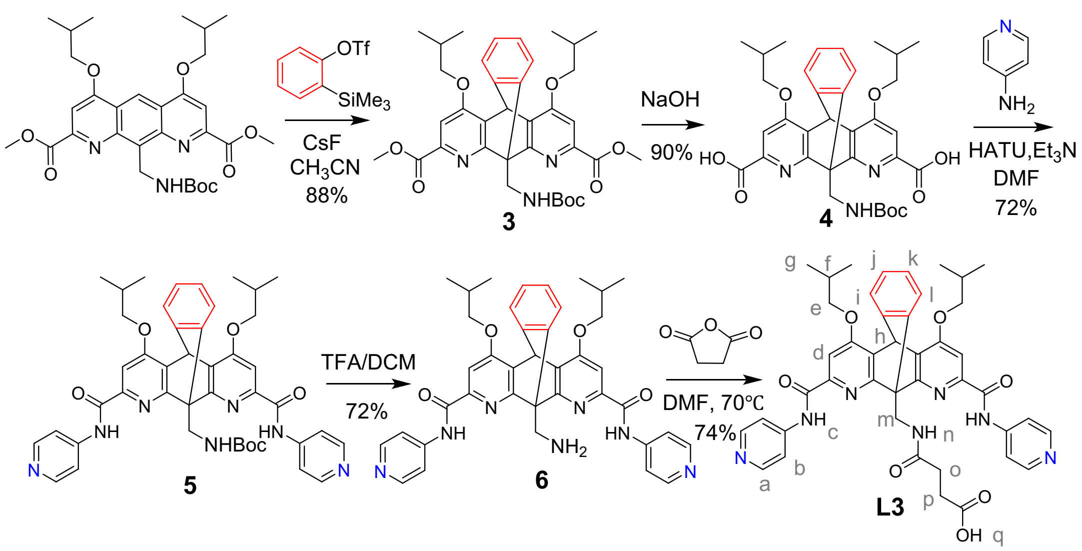

Scheme 2 | *Synthetic procedures for ligands **L3**.*

Citation: *CCS Chem.* **2023**, Just Published. DOI: 10.31635/ccschem.023.202302940
Link to VoR: https://doi.org/10.31635/ccschem.023.202302940

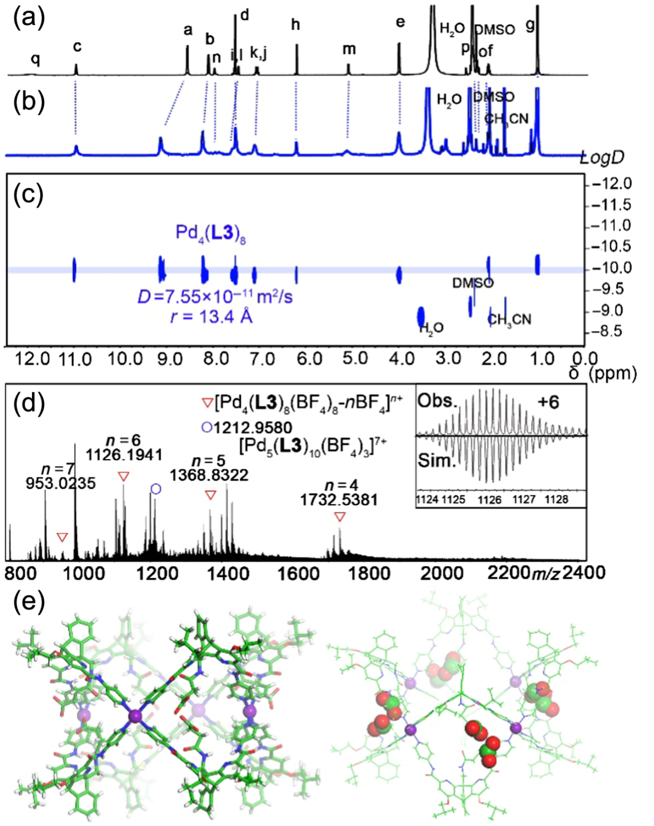

Figure 6 | *^{1}H NMR spectra (500 MHz, DMSO-d_6, 298 K) of ^{1}H NMR spectra of (a)* ***L3*** *and (b) its self-assembly product Pd$_4$(**L3**)$_8$. (c) The DOSY spectra of Pd$_4$(**L3**)$_8$. (d) ESI-TOF-MS for Pd$_4$(**L3**)$_8$ as its BF_4^- salt. Inset shows the comparison of the observed isotopic pattern with the simulated spectrum. (e) X-ray crystal structure of Pd$_4$(**L3**)$_8$ with side views (left) and highlights the 9-position endohedral carboxylic acids (right). Solvent molecules and counterions are omitted for clarity.*

9-methyl in the precursor 1,8-diazaanthracene-2,7-dicarboxylate ester could be easily functionalized into a Boc-protected 9-methylamino diazaanthracene derivative.[73] Next, triptycene formation and installation of the pyridine coordination sites were performed in a manner analogous to **L2**. Subsequent amine deprotection and reaction with succinic anhydride allowed the incorporation of the carboxylic acid group in **L3**.

Despite potential for the endohedral carboxylic acid to compete with metal-pyridine interactions or to act as a hydrogen bond acceptor and donor with the amides and thus limit the conformational constraints,[15,74,75] self-assembly with **L3** proceeded without any problems. Upon reaction of **L3** with Pd^{2+} (NO_3^-, BF_4^-, $CF_3SO_3^-$, or PF_6^- salt), in a 2:1 molar ratio in DMSO-d_6 or DMF-d_7, similar changes as for self-assembly with **L2**, that is, a single set of signals shifted relative to the free ligand, are observed by ^{1}H NMR (Figure 6a,b and Supporting Information Figures S16–S19, S95, and S96). Given the similar bend

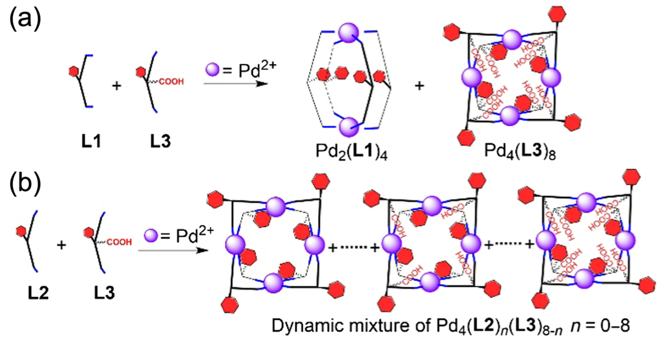

Figure 7 | *Mixed ligands self-assembly with ligand* ***L3****, mixed with (a)* ***L1*** *leads to narcissistic self-sorting of M$_2$(**L1**)$_4$ and M$_4$(**L3**)$_8$ assemblies and (b)* ***L2*** *formed nonsorted scrambled dynamic mixtures of Pd$_4$(**L2**)$_n$(**L3**)$_{8-n}$(BF$_4$)$_8$, n = 0–8.*

angles expected for **L2** and **L3**, self-assembly with the functionalized ligand should also lead to an M_4L_8 structure. This was supported by DOSY studies (D = 7.55x10^{-11} m^2/s; r = 13.4 Å), which suggested the formation of a complex with a size similar to parent Pd$_4$(**L2**)$_8^{8+}$ (Figure 6c and Supporting Information Figure S27). The Pd$_4$(**L3**)$_8$(BF$_4$)$_8$ formula was further confirmed by ESI-TOF-MS, though some low-intensity signals for an M_5L_{10} structure could also be observed (Figure 6d and Supporting Information Figures S44–S50). The presence of the more bulky group on the 9-position of **L3** relative to **L2** may lead to this minor formation of some of the larger macrocycles.[76] Still, the species observed by NMR represents >90% of ligands used for self-assembly. Additionally, the X-ray crystal structure of the product showed Pd$_4$(**L3**)$_8^{8+}$ and was highly similar to the M$_4$(**L2**)$_8^{8+}$ structure (Figure 6e). The 9-position substituents are still found pointing into the cavity and oriented toward each other such that they occupy the cavity windows formed by the pairs of bridging ligands. This also leads to short distances between neighboring carboxylic acid groups (O–O distances of 2.3–2.7 Å), suggesting potential hydrogen bond formation between these groups. Such interactions might be expected to lead to some preference for self-sorting. However, self-assembly with mixtures of **L3** and **L2** resulted in statistical mixtures of M_4L_8 species with different ratios of the two ligands, though similar studies using **L3** and **L1** still showed self-sorting into M$_2$(**L1**)$_4^{4+}$ and M$_4$(**L3**)$_8^{8+}$ based on the different bend angles (Figure 7a,b and Supporting Information Figures S21–S24).

Conclusion

We have provided an effective strategy for controlling palladium-based self-assembly with flexible and nonplanar ligands by combining endohedral noncovalent interactions in aromatic amides with additional shape complementarity brought by a dual curvature in the ligand. Three asymmetric diazatryptycene amide-based ligands were synthesized and used for self-assembly with Pd^{2+}. Impressively, the constraints designed into the ligands provide high stereoselectivity for the self-assembly process, leading to only a single M_2L_4 cage (**L1**) or M_4L_8 double-walled metallomacrocycle (**L2** or **L3**) out of all of the possible stereoisomers. Moreover, we show that despite the flexibility around the amide groups in the ligands, the noncovalent interactions arranged on the ligand backbone provide excellent control over the ligand bend angle, allowing narcissistic self-sorting in mixtures of ligands with different bend angles. This demonstrated level of structural control and the high modularity afforded by the amide connectivity can allow rapid access to libraries of diversely functionalized ligands for applications in sensing and catalysis. To highlight this versatility, we show that this strategy can be used to generate endohedrally functionalized M_4(**L3**)$_8$ structures with deep cavities lined with competitive functional groups. These results provide promising new design strategies for coordination-driven self-assembly where additional shape complementarity between dually curved ligands can be used for the formation of asymmetric functionalized cavities of interest for diverse applications.

Supporting Information

Supporting Information is available and includes full experimental details, including synthetic procedures and spectroscopic data for ligands **L1**–**L3** and their corresponding cages. CCDC 2121219 Pd_2(**L1**)$_4$, 2121220 Pd_4(**L2**)$_8$, and 2111410 Pd_4(**L3**)$_8$ contain the supplementary crystallographic data for this paper. The data can be obtained free of charge from The Cambridge Crystallographic Data Centre via www.ccdc.cam.ac.uk/structures.

Conflict of Interest

There is no conflict of interest to report.

Funding Information

This research was supported in part through the Concerted Research Action (ARC16/21-074) and the China Scholarship Council (pre-doctoral fellowships for C.-L.L.). Computational resources were provided by the supercomputing facilities of the Université catholique de Louvain (CISM/UCL) and the Consortium des équipements de Calcul Intensif en Fédération Wallonie Bruxelles (CPCI) funded by the Fond de la Recherche Scientifique de Belgique (F.R.S.-FNRS) under convention 2.5020.11. We thank Dr. S. Ouk for his generous financial support through the Fondation Louvain.

Preprint Statement

Research presented in this article was posted on a preprint server prior to publication in *CCS Chemistry*. The corresponding preprint article can be found here: (10.26434/chemrxiv-2021-4z45w-v3; https://chemrxiv.org/engage/chemrxiv/article-details/629f1b272e6269c3f07a518f).

Acknowledgments

The authors wish to acknowledge Dr. Gabriella Barozzino for help with NMR measurements.

References

1. Heckmann, C. M.; Paradisi, F. Looking Back: A Short History of the Discovery of Enzymes and How They Became Powerful Chemical Tools. *ChemCatChem* **2020**, *12*, 6082–6102.
2. Drout, R. J.; Robison, L.; Farha, O. K. Catalytic Applications of Enzymes Encapsulated in Metal–Organic Frameworks. *Coord. Chem. Rev.* **2019**, *381*, 151–160.
3. Benkovic, S. J.; Hammes-Schiffer, S. A Perspective on Enzyme Catalysis. *Science* **2003**, *301*, 1196–1202.
4. Liu, Y.; Zhao, W.; Chen, C. H.; Flood, A. H. Chloride Capture Using a C-H Hydrogen-Bonding Cage. *Science* **2019**, *365*, 159–161.
5. Liu, Z.; Nalluri, S. K. M.; Stoddart, J. F. Surveying Macrocyclic Chemistry: From Flexible Crown Ethers to Rigid Cyclophanes. *Chem. Soc. Rev.* **2017**, *46*, 2459–2478.
6. Kim, D. S.; Sessler, J. L. Calix[4]pyrroles: Versatile Molecular Containers with Ion Transport, Recognition, and Molecular Switching Functions. *Chem. Soc. Rev.* **2015**, *44*, 532–546.
7. Gil-Ramírez, G.; Leigh, D. A.; Stephens, A. J. Catenanes: Fifty Years of Molecular Links. *Angew. Chem. Int. Ed.* **2015**, *54*, 6110–6150.
8. Lindoy, L. F.; Park, K.-M.; Lee, S. S. Metals, Macrocycles and Molecular Assemblies – Macrocyclic Complexes in Metallo-Supramolecular Chemistry. *Chem. Soc. Rev.* **2013**, *42*, 1713–1727.
9. Cook, T. R.; Zheng, Y.-R.; Stang, P. J. Metal–Organic Frameworks and Self-Assembled Supramolecular Coordination Complexes: Comparing and Contrasting the Design, Synthesis, and Functionality of Metal–Organic Materials. *Chem. Rev.* **2013**, *113*, 734–777.
10. Kondratuk, D. V.; Perdigao, L. M. A.; O'Sullivan, M. C.; Svatek, S.; Smith, G.; O'Shea, J. N.; Beton, P. H.; Anderson, H. L. Two Vernier-Templated Routes to a 24-Porphyrin Nanoring. *Angew. Chem. Int. Ed.* **2012**, *51*, 6696–6699.
11. Tozawa, T.; Jones, J. T. A.; Swamy, S. I.; Jiang, S.; Adams, D. J.; Shakespeare, S.; Clowes, R.; Bradshaw, D.; Hasell T.; Chong, S. Y.; Tang, C.; Thompson, S.; Parker, J.; Trewin, A.; Bacsa, J.; Slawin, A. M. Z.; Steiner, A.; Cooper, A. I. Porous Organic Cages. *Nat. Mater.* **2009**, *8*, 973–978.

12. MacGillivray, L. R.; Atwood, J. L. A Chiral Spherical Molecular Assembly Held Together by 60 Hydrogen Bonds. *Nature* **1997**, *389*, 469–472.
13. Zou, Y.-Q.; Zhang, D.; Ronson, T. K.; Tarzia, A.; Lu, Z.; Jelfs, K. E.; Nitschke, J. R. Sterics and Hydrogen Bonding Control Stereochemistry and SelfSorting in BINOL-Based Assemblies. *J. Am. Chem. Soc.* **2021**, *143*, 9009–9015.
14. Percástegui, E. G.; Ronson, T. K.; Nitschke, J. R. Design and Applications of Water-Soluble Coordination Cages. *Chem. Rev.* **2020**, *120*, 13480–13544.
15. Gosselin, A. J.; Rowland, C. A.; Bloch, E. D. Permanently Microporous Metal–Organic Polyhedra. *Chem. Rev.* **2020**, *120*, 8987–9014.
16. Sun, Y.; Chen, C.; Stang, P. J. Soft Materials with Diverse Suprastructures via the Self-Assembly of Metal–Organic Complexes. *Acc. Chem. Res.* **2019**, *52*, 802–817.
17. Saha, S.; Regeni, I.; Clever, G. H. Structure Relationships Between bis-Monodentate Ligands and Coordination Driven Self-Assemblies. *Coord. Chem. Rev.* **2018**, *374*, 1–14.
18. Cook, T. R.; Stang, P. J. Recent Developments in the Preparation and Chemistry of Metallacycles and Metallacages via Coordination. *Chem. Rev.* **2015**, *115*, 7001–7045.
19. Fujita, D.; Ueda, Y.; Sato, S.; Yokoyama, H.; Mizuno, N.; Kumasaka, T.; Fujita, M. Self-Assembly of $M_{30}L_{60}$ Icosidodecahedron. *Chem* **2016**, *1*, 91–101.
20. Fujita, D.; Ueda, Y.; Sato, S.; Mizuno, N.; Kumasaka, T.; Fujita, M. Self-Assembly of Tetravalent Goldberg Polyhedra from 144 Small Components. *Nature* **2016**, *540*, 563–566.
21. Harris, K.; Fujita, D.; Fujita, M. Giant Hollow M_nL_{2n} Spherical Complexes: Structure, Functionalisation and Applications. *Chem. Commun.* **2013**, *49*, 6703–6712.
22. Zhang, D.; Ronson, T. K.; Zou, Y.-Q.; Nitschke, J. R. Metal–Organic Cages for Molecular Separations. *Nat. Rev. Chem.* **2021**, *5*, 168–182.
23. Yadav, S.; Kannan, P.; Qiu, G. Cavity-Based Applications of Metallo-Supramolecular Coordination Cages (MSCCs). *Org. Chem. Front.* **2020**, *7*, 2842–2872.
24. Zhang, M.; Saha, M. L.; Wang, M.; Zhou, Z.; Song, B.; Lu, C.; Yan, X.; Li, X.; Huang, F.; Yin, S.; Stang, P. J. Multicomponent Platinum(II) Cages with Tunable Emission and Amino Acid Sensing. *J. Am. Chem. Soc.* **2017**, *139*, 5067–5074.
25. Casini, A.; Woods, B.; Wenzel, M. The Promise of Self-Assembled 3D Supramolecular Coordination Complexes for Biomedical Applications. *Inorg. Chem.* **2017**, *56*, 14715–14729.
26. Wang, Q.-Q.; Gonell, S.; Leenders, S. H. A. M.; Dürr, M.; Ivanović-Burmazović, I.; Reek, J. N. H. Self-Assembled Nanospheres with Multiple Endohedral Binding Sites Pre-Organize Catalysts and Substrates for Highly Efficient Reactions. *Nat. Chem.* **2016**, *8*, 225–230.
27. Brown, C. J.; Toste, F. D.; Bergman, R. G.; Raymond, K. N. Supramolecular Catalysis in Metal–Ligand Cluster Hosts. *Chem. Rev.* **2015**, *115*, 3012–3035.
28. Wang, J.; He, C.; Wu, P.; Wang, J.; Duan, C. An Amide-Containing Metal–Organic Tetrahedron Responding to a Spin-Trapping Reaction in a Fluorescent Enhancement Manner for Biological Imaging of NO in Living Cells. *J. Am. Chem. Soc.* **2011**, *133*, 12402–12405.
29. Mal, P.; Breiner, B.; Rissanen, K.; Nitschke, J. R. White Phosphorus Is Air-Stable Within a Self-Assembled Tetrahedral Capsule. *Science* **2009**, *324*, 1697–1699.
30. Dill, K. A.; MacCallum, J. L. The Protein-Folding Problem, 50 Years on. *Science* **2012**, *338*, 1042–1046.
31. Hartl, F. U.; Bracher, A.; Hayer-Hartl, M. Molecular Chaperones in Protein Folding and Proteostasis. *Nature* **2011**, *475*, 324–332.
32. Seidel, S. R.; Stang, P. J. High-Symmetry Coordination Cages via Self-Assembly. *Acc. Chem. Res.* **2002**, *35*, 972–983.
33. Yoshizawa, M.; Catti, L. Bent Anthracene Dimers as Versatile Building Blocks for Supramolecular Capsules. *Acc. Chem. Res.* **2019**, *52*, 2392–2404.
34. Yue, N. L. S.; Eisler, D. J.; Jennings, M. C.; Puddephatt, R. J. Macrocyclic and Lantern Complexes of Palladium(II) with Bis(amidopyridine) Ligands: Synthesis, Structure, and Host–Guest Chemistry. *Inorg. Chem.* **2004**, *43*, 7671–7681.
35. Lewis, J. E. M.; Crowley, J. D. Metallo-Supramolecular Self-Assembly with Reduced-Symmetry Ligands. *ChemPlusChem* **2020**, *85*, 815–827.
36. Tessarolo, J.; Lee, H.; Sakuda, E.; Umakosh, i. K.; Clever, G. H. Integrative Assembly of Heteroleptic Tetrahedra Controlled by Backbone Steric Bulk. *J. Am. Chem. Soc.* **2021**, *143*, 6339–6344.
37. Sudan, S.; Li, R.-J.; Jansze, S. M.; Platzek, A.; Rudolf, R.; Clever, G. H.; Fadaei-Tirani, F.; Scopelliti, R.; Severin, K. Identification of a Heteroleptic $Pd_6L_6L'_6$ Coordination Cage by Screening of a Virtual Combinatorial Library. *J. Am. Chem. Soc.* **2021**, *143*, 1773–1778.
38. Pullen, S.; Tessarolo, J.; Clever, G. H. Increasing Structural and Functional Complexity in Self-Assembled Coordination Cages. *Chem. Sci.* **2021**, *12*, 7269–7293.
39. Saha, S.; Holzapfel, B.; Chen, Y.-T.; Terlinden, K.; Lill, P.; Gatsogiannis, C.; Rehage, H.; Clever, G. H. Rational Design of an Amphiphilic Coordination Cage-Based Emulsifier. *J. Am. Chem. Soc.* **2018**, *140*, 17384–17388.
40. Pullen, S.; Clever, G. H. Mixed-Ligand Metal–Organic Frameworks and Heteroleptic Coordination Cages as Multifunctional Scaffolds—A Comparison. *Acc. Chem. Res.* **2018**, *51*, 3052–3064.
41. Bloch, W. M.; Abe, Y.; Holstein, J. J.; Wandtke, C. M.; Dittrich, B.; Clever, G. H. Geometric Complementarity in Assembly and Guest Recognition of a Bent Heteroleptic cis-$[Pd_2LA_2LB_2]$ Coordination Cage. *J. Am. Chem. Soc.* **2016**, *138*, 13750–13755.
42. Kryschenko, Y. K.; Seidel, S. R.; Muddiman, D. C.; Nepomuceno, A. I.; Stang, P. J. Coordination-Driven Self-Assembly of Supramolecular Cages: Heteroatom-Containing and Complementary Trigonal Prisms. *J. Am. Chem. Soc.* **2003**, *125*, 9647–9652.
43. Freye, S.; Michel, R.; Stalke, D.; Pawliczek, M.; Frauendorf, H.; Clever, G. H. Template Control over Dimerization and Guest Selectivity of Interpenetrated Coordination Cages. *J. Am. Chem. Soc.* **2013**, *135*, 8476–8479.
44. Li, R.-J.; Marcus, A.; Fadaei-Tirani, F.; Severin, K. Orientational Self-Sorting: Formation of Structurally Defined

Citation: *CCS Chem.* **2023**, Just Published. DOI: 10.31635/ccschem.023.202302940
Link to VoR: https://doi.org/10.31635/ccschem.023.202302940

Pd_4L_8 and Pd_6L_{12} Cages from Low-Symmetry Dipyridyl Ligands. *Chem. Commun.* **2021**, *57*, 10023–10026.
45. Zhu, R.; Bloch, W. M.; Holstein, J. J.; Mandal, S.; Schafer, L. V.; Clever, G. H. Donor-Site-Directed Rational Assembly of Heteroleptic cis-[$Pd_2L_2L'_2$] Coordination Cages from Picolyl Ligands. *Chem. Euro. J.* **2018**, *24*, 12976–12982.
46. Klein, C.; Gutz, C.; Bogner, M.; Topic, F.; Kiassanen, K.; Lutzen, A. A New Structural Motif for an Enantiomerically Pure Metallosupramolecular Pd_4L_8 Aggregate by Anion Templating. *Angew. Chem. Int. Ed.* **2014**, *53*, 3739–3742.
47. Lewis, J. E. M. Multi-Functional, Low Symmetry Pd_2L_4 Nanocage Libraries. *Chem. Eur. J.* **2021**, *27*, 4454–4460.
48. Mishra, S. S.; Kompella, S. V. K.; Krishnaswamy, S.; Balasubramanian, S.; Chand, D. K. Low-Symmetry Self-Assembled Coordination Complexes with Exclusive Diastereoselectivity: Experimental and Computational Studies. *Inorg. Chem.* **2020**, *59*, 12884–12894.
49. Lisboa, L. S.; Findlay, J. A.; Wright, L. J.; Hartinger, C. G.; Crowley, J. D. A Reduced-Symmetry Heterobimetallic $[PdPtL_4]^{4+}$ Cage: Assembly, Guest Binding, and Stimulus-Induced Switching. *Angew. Chem. Int. Ed.* **2020**, *59*, 11101–11107.
50. Lewis, J. E. M.; Tarzia, A.; White, A. J. P.; Jelfs, K. E. Conformational Control of Pd_2L_4 Assemblies with Unsymmetrical Ligands. *Chem. Sci.* **2020**, *11*, 677–683.
51. Chen, B.; Horiuchi, S.; Holstein, J. J.; Tessarolo, J.; Clever, G. H. Tunable Fullerene Affinity of Cages, Bowls and Rings Assembled by Pd^{II} Coordination Sphere Engineering. *Chem. Eur. J.* **2019**, *25*, 14921–14927.
52. Preston, D.; Barnsley, J. E.; Gordon, K. C.; Crowley, J. D. Controlled Formation of Heteroleptic $[Pd_2(La)_2(Lb)_2]^{4+}$ Cages. *J. Am. Chem. Soc.* **2016**, *138*, 10578–10585.
53. Löffler, S.; Lübben, J.; Wuttke, A.; Mata, R. A.; John, M.; Dittrich, B.; Clever, G. H. Internal Dynamics and Guest Binding of a Sterically Overcrowded Host. *Chem. Sci.* **2016**, *7*, 4676–4684.
54. Walker, S. E.; Boer, S. A.; Malcomson, T.; Paterson, M. J.; Tuck, K. L.; Turner, D. R. Steric Control of Sorting Regimes in Self-Assembled Cages. *Chem. Commun.* **2021**, 57, 12456–12459.
55. Vasdev, R. A. S.; Preston, D.; Casey-Stevens, C. A.; Marti-Centelles, V.; Lusby, P. J.; Garden, A. L.; Crowley, J. D. Exploiting Supramolecular Interactions to Control Isomer Distributions in Reduced-Symmetry $[Pd_2L_4]^{4+}$ Cages. *Inorg. Chem.* **2023**, *62*, 1833–1844.
56. Sawada, T.; Fujita, M. Orderly Entangled Nanostructures of Metal–Peptide Strands. *Bull. Chem. Soc. Jpn.* **2021**, *94*, 2342.
57. Inomata, Y.; Sawada, T.; Fujita, M. Metal-Peptide Torus Knots from Flexible Short Peptides. *Chem* **2020**, 6, 294–303.
58. Sawada, T.; Inomata, Y.; Shimokawa, K.; Fujita, M. A Metal–Peptide Capsule by Multiple Ring Threading. *Nat. Commun.* **2019**, 10, 5687.
59. Yamagami, M.; Sawada, T.; Fujita, M. Synthetic β-Barrel by Metal-Induced Folding and Assembly. *J. Am. Chem. Soc.* **2018**, 140, 8644.
60. Liu, C.-L.; Bobylev, E. O.; Fu, Y.; Poole, D. A.; Robeyns, K.; Fustin, C.-A.; Garcia, Y.; Reek, J. N. H.; Singleton, M. L. Balancing Ligand Flexibility Versus Rigidity for the Stepwise Self-Assembly of $M_{12}L_{24}$ via M_6L_{12} Metal-Organic Cages. *Chem. Eur. J.* **2020**, *26*, 11960–11965.
61. Berni, E.; Kauffmann, B.; Bao, C.; Lefeuvre, J.; Bassani, D. M.; Huc, I. Assessing the Mechanical Properties of a Molecular Spring. *Chem. Eur. J.* **2007**, *13*, 8463–8469.
62. Kerff, F.; Liu, C.-L.; Mu, X.; Gilbert, U.; Smal, L.; Meinertzhagen, L.; Kauffmann, B.; Robeyns, K.; Singleton, M. L. Functionalized 1,8-Diazaiptycenes as Monomers for Aromatic Oligoamide Foldamers. *ChemPlusChem* **2021**, *86*, 1162–1166.
63. Frisch, M. J.; Trucks, G. W.; Schlegel, H. B.; Scuseria, G. E.; Robb, M. A.; Cheeseman, J. R.; Scalmani, G.; Barone, V.; Mennucci, B.; Petersson, G. A.; Nakatsuji, H.; Caricato, M.; Li, X.; Hratchian, H. P.; Izmaylov, A. F.; Bloino, J.; Zheng, G.; Sonnenberg, J. L.; Hada, M.; Ehara, M.; Toyota, K.; Fukuda, R.; Hasegawa, J.; Ishida, M.; Nakajima, T.; Honda, Y.; Kitao, O.; Nakai, H.; Vreven, T.; Montgomery, J. A., Jr.; Peralta, J. E.; Ogliaro, F.; Bearpark, M.; Heyd, J. J.; Brothers, E.; Kudin, K. N.; Staroverov, V. N.; Keith, T.; Kobayashi, R.; Normand, J.; Raghavachari, K.; Rendell, A.; Burant, J. C.; Iyengar, S. S.; Tomasi, J.; Cossi, M.; Rega, N.; Millam, J. M.; Klene, M.; Knox, J. E.; Cross, J. B.; Bakken, V.; Adamo, C.; Jaramillo, J.; Gomperts, R.; Stratmann, R. E.; Yazyev, O.; Austin, A. J.; Cammi, R.; Pomelli, C.; Ochterski, J. W.; Martin, R. L.; Morokuma, K.; Zakrzewski, V. G.; Voth, G. A.; Salvador, P.; Dannenberg, J. J.; Dapprich, S.; Daniels, A. D.; Farkas, O.; Foresman, J. B.; Ortiz, J. V.; Cioslowski, J.; Fox, D. J. *Gaussian 09, Revision D.01*; Gaussian, Inc.: Wallingford, CT, **2013**.
64. CrystalClear-SM Expert 2.1 (Rigaku 2013) Software, Version 5.6.2.0, Tokyo, Japan.
65. Sheldrick, G. M. Crystal Structure Refinement with SHELXL. *Acta Crystallogr. Sect. C: Struct. Chem.* **2015**, *71*, 3–8.
66. Burla, M. C.; Caliandro, R.; Camalli, M.; Carrozzini, B.; Cascarano, G. L.; De Caro, L.; Giacovazzo, C.; Polidori, G.; Spagna, R. An Improved Tool for Crystal Structure Determination and Refinement. *J. Appl. Crystallogr.* **2005**, *38*, 381–388.
67. CrysAlisPRO Software System, Vol. Rigaku Corporation: Oxford, UK, **2015**.
68. Sheldrick, G. M. SHELXT - Integrated Space-Group and Crystal-Structure Determination. *Acta Crystallogr., Sect. A: Found. Adv.*, **2015**, *71*, 3–8.
69. Jansze, S. M.; Cecot, G.; Wise, M. D.; Zhurov, K. O.; Ronson, T. K.; Castilla, A. M.; Finelli, A.; Pattison, P.; Solari, E.; Scopelliti, R.; Zelinskii, G. E.; Vologzhanina, A. V.; Voloshin, Y. Z.; Nitschke, J. R.; Severin, K. Ligand Aspect Ratio as a Decisive Factor for the Self-Assembly of Coordination Cages. *J. Am. Chem. Soc.* **2016**, *138*, 2046–2054.
70. Johnson, A. M.; Wiley, C. A.; Young, M. C.; Zhang, X.; Lyon, Y.; Julian, R. R.; Hooley, R. J. Narcissistic Self-Sorting in Self-Assembled Cages of Rare Earth Metals and Rigid Ligands. *Angew. Chem. Int. Ed.* **2015**, *54*, 5641–5645.
71. Sun, Q.-F.; Iwasa, J.; Ogawa, D.; Ishido, Y.; Sato, S.; Ozeki, T.; Sei, Y.; Yamaguchi, K.; Fujita, M. Self-Assembled $M_{24}L_{48}$ Polyhedra and Their Sharp Structural Switch Upon Subtle Ligand Variation. *Science* **2010**, *328*, 1144–1147.
72. Bogie, P. M.; Miller, T. F.; Hooley, R. J. Synthesis and Applications of Endohedrally Functionalized Metal-Ligand Cage Complexes. *Isr. J. Chem.* **2019**, *59*, 130–139.
73. Singleton, M. L.; Castellucci, N.; Massip, S.; Kauffmann, B.; Ferrand, Y.; Huc, I. Synthesis of 1,8-Diazaanthracenes as

Building Blocks for Internally Functionalized Aromatic Oligoamide Foldamers. *J. Org. Chem.* **2014**, *79*, 2115–2122.
74. Fang, Y.; Powell, J. A.; Li, E.; Wang, Q.; Perry, Z.; Kirchon, A.; Yang, X.; Xiao, Z.; Zhu, C.; Zhang, L.; Huang, F.; Zhou, H.-C. Catalytic Reactions Within the Cavity of Coordination Cages. *Chem. Soc. Rev.* **2019**, *48*, 4707–4730.
75. Lee, J.; Farha, O. K.; Roberts, J.; Scheidt, K. A.; Nguyen, S. T.; Hupp, J. T. Metal–Organic Framework Materials as Catalysts. *Chem. Soc. Rev.* **2009**, *38*, 1450–1459.
76. Bobylev, E. O.; Poole, D. A., III; de Bruin, B.; Reek, J. N. H. Selective Formation of $Pt_{12}L_{24}$ Nanospheres by Ligand Design. *Chem. Sci.* **2021**, *12*, 7696–7705.

Citation: *CCS Chem.* **2023**, Just Published. DOI: 10.31635/ccschem.023.202302940
Link to VoR: https://doi.org/10.31635/ccschem.023.202302940